

## **Chapter 2. Molecular dynamics simulation of planar elongational flow at constant pressure and temperature.**

*After an introduction to common laboratory techniques and a review of experimental and numerical results for the viscosity of liquids under extensional flows, an implementation of the Nosé-Hoover method for constant pressure in conjunction with a Gaussian thermostat mechanism for constant temperature is proposed for planar elongation. Accurate results for the viscosity of simple atomic liquids are shown.*

### ***2.1. Relevance of extensional flows.***

The two main kinds of flows used to characterize the viscoelastic properties of liquids are commonly labelled as shear and shear-free flows (Bird *et al.*, 1987). In the latter, planar elongation is one of the possible combinations among the broader class of extensional flows, the others being, for instance, uniaxial or biaxial flows. These irrotational geometries have a great importance in a number of applications in industrial sectors, such as those involved with polymer melts and glass technology, lubrication or oil-related processes. Typical manufacturing methods such as film-blowing, injection-molding, fiber-spinning and sheet-casting involve the compression of a fluid sample in one direction and the dilation in one or more. So, it is understandable that there is still a great deal of effort devoted to characterizing materials under shear-free flows with the aid of experimental techniques and modelling them with physical descriptions at various levels, such as through constitutive equations or finite elements methods.

From a scientific point of view, the rheology of extensional flows poses a spectrum of interesting problems. A complete review of them is beyond the scope of this Chapter, which is focussed on the discussion of major viscoelastic properties, both from experimental and theoretical points of view. A good overview on active research approaches and open questions about general problems in rheology can be found in a special issue of the Journal of Non-Newtonian Fluid Mechanics (Roberts and McKinley, 2006), where a comprehensive perspective on the state-of-the-art of the research on extensional flows is given.

---

## 2. Molecular dynamics simulation of planar elongational flow at constant pressure and temperature

---

In the following, we are interested in discussing the most common techniques for laboratory measurements of steady-state elongational viscosities of liquid systems, with a particular emphasis on polymer melts and solutions. This is because these are the natural candidates for future applications of the *new-cell* algorithm we present in Section 2.3, which allows the simulation of PEF for systems kept at constant temperature and pressure, as happens in the most common experimental settings discussed below.

## ***2.2. Experimental results on the viscosity of liquids under extensional flows.***

The interest towards the rheological response of fluids under extensional flows can be dated back to the beginning of last century, with the two seminal contributions by Trouton (Trouton, 1906) and Fano (Fano, 1908). An historical overview on this and other themes in rheology can be found in a dedicated book (Tanner and Walters, 1999), whereas two recent comprehensive reviews represent the starting point for this study (Petrie, 2006b; 2006a). In modern times, the key role of these flows for industrial practice spurred the first works on polymer melts in the 1960s, which in fact came from scientists working in private laboratories like Cogswell (Cogswell, 1968), Ballman (Ballman, 1965) and Meissner (Meissner, 1969) and were primarily interested in measuring the dependency of material stress on strain rate. Around the same time, the deep work by Vinogradov in the Soviet Union was the only acknowledged academic contribution (Vinogradov *et al.*, 1970a; Vinogradov *et al.*, 1970b). His broader range of interests also included profound ideas like the separation of viscous and plastic contributions to the strain (Vinogradov and Malkin, 1979): a recurrent theme in rheology which dates back to Trouton, Rankine (Trouton and Rankine, 1904), Fano and Bingham (Bingham, 1924) among others.

Nowadays, experiments on the rheometry of fluids subject to stretching flows are carried out worldwide, with the use of more and more sophisticated techniques. In general, the different types of experimental procedures can be grouped into four main categories (James and Walters, 1994; Petrie, 1995): the tensile test and the filament stretching rheometer, fibre spinning, stagnation point flows or opposite jets, and converging and contraction flows. Other approaches that are not described here are those which employ the methods of bubble inflation (Joye *et al.*, 1972; Denson and Crady, 1973; Han and Park, 1975), flows past rigid spheres (Bagchi and Balachandar, 2002) and cylinders (McKinley *et al.*, 1993), and other hybrid methods. Interested readers can ‘watch’ an introduction with many examples in McKinley’s group website (McKinley, 2007).

Before analysing these arrangements in some detail, a brief treatment of some general aspects related to the measurement of viscosity in elongational flows is needed.

As we said, depending on the combination of compressing and dilating contributions in the flow, different types of perturbations are possible. If  $\mathbf{D}$  is the diagonal strain rate tensor and  $\dot{\epsilon}$  is the constant rate of strain, then the most commonly defined flows are (Dealy, 1994): uniaxial extension for  $D_{11} = \dot{\epsilon}$  and  $D_{22} = D_{33} = -\frac{1}{2}\dot{\epsilon}$ , biaxial extension for  $D_{11} = D_{22} = \dot{\epsilon}$  and  $D_{33} = -2\dot{\epsilon}$ , and planar elongation for the familiar  $D_{11} = \dot{\epsilon}$ ,  $D_{22} = -\dot{\epsilon}$  and  $D_{33} = 0$ . There are other geometries when  $D_{11} = \dot{\epsilon}$ ,  $D_{22} = m\dot{\epsilon}$  and  $D_{33} = -(1+m)\dot{\epsilon}$ , with  $-0.5 \leq m \leq 1$ , which have received some attention (Demarmels and Meissner, 1985, 1986). The established definition of elongational viscosity or *tensile* viscosity applied to uniaxial flows, which is also the one initially proposed in 1906 by Trouton, is as follows: given the stress tensor  $\boldsymbol{\sigma}$  and defined the net tensile stress as  $\sigma_E = \sigma_{11} - \sigma_{22}$ , the elongational viscosity is then given by

$$\eta_T(\dot{\epsilon}) = \lim_{t \rightarrow \infty} \frac{\sigma_E(t, \dot{\epsilon})}{\dot{\epsilon}} \quad (2.1)$$

From an operational point of view, it should be clear that this definition is rather poor. The conditions it assumes are almost impractical to realize in the laboratory: the flow must be both steady and spatially uniform, the stress must have settled down to some constant value within the time of experiment, the sample must not reach its maximum strain beyond which it becomes irregular or breaks, the strain must also be (reasonably) constant over large part of the sample, etc. Moreover, it should be noted that the above definition does not consider corrections due to surface tension, which are crucial in some type of settings like fibre spinning and must be evaluated and subtracted from (2.1).

Because these assumptions are difficult to achieve experimentally, much confusion has arisen in the literature about extensional viscosity (Petrie, 2006a). In practice, actual measurements extract what is more appropriately defined *transient* extensional viscosity, or an approximation of tensile viscosity in time and space under certain, explicitly stated, assumptions. In some sense this is not even a compromise: transient viscosity is indeed the quantity of interest in the majority of industrial processes, where flows are never steady and spatially uniform.

For its geometry, extensional flow cannot be imposed in a way that it is steady both in the Eulerian description, i.e. the one that records the succession of fluid parcels passing past a point in space, and the Lagrangian description, i.e. the one that follows all individual fluid parcels as their motion unravels with time, except in one symmetric point called the *stagnation* point (Petrie, 1979). In practice, this means that a steady flow can either be reproduced in the laboratory frame of reference and the sample undergoes a changing strain rate (such as in fibre spinning, contraction flows or opposite jets) or have a constant strain rate while the material is changing position (like in the tensile test).

Let us now describe the different techniques for polymer melts and solutions in some detail. As said, these settings can be allocated into four main groups:

- Tensile tests and the filament stretching rheometers. The basic idea of the first is that a rod-like sample is stretched by the action of one or more cylinders, which can be mechanically or electrically controlled to generate different extensional geometries, depending on their spatial arrangement. Care must be taken in using cylinders that are extended as uniformly as possible, so that flows are homogeneous. Accurate descriptions of the various combinations and their range of application for polymer melts can be found in the review by Meissner (Meissner, 1985) and in the book by Dealy (Dealy, 1982), among others. The use of rotary clamps that grip ‘new’ material in the sample improves the steadiness and homogeneity of the flow, avoiding the appearance of ‘necks’ (Meissner *et al.*, 1981; Meissner and Hoestettler, 1994). In the filament stretching rheometer, the fluid is placed between two plates which are separated in a way such that an almost homogeneous uniaxial elongation is achieved. Mechanical and optical measurements are made at the central plane of symmetry to determine the stress response and the molecular conformation of the sample (McKinley and Sridhar, 2002). The reliability of this method depends on the balance of capillary, viscous and elastic effects, which are all crucial to maintain the sample in an almost cylindrical shape and avoid end-effects (Spiegelberg *et al.*, 1996). Whereas this method is suitable for moderately viscous materials, like polymer solutions, tensile tests are used for more viscous liquids, like polymer melts.

- Fibre spinning. In this type of setting, the fluid is usually pumped through a tube and drawn into a *spinline* by means of a rotating drum, so that in every point inside the sample there is an extending force in one direction and a compressing contribution in two perpendicular directions (Gupta and Sridhar, 1998; Hinch, 2003). For moderately viscous samples, the drawing force can also be gravity, and the fluid stretches under its own weight (Patel and Bogue, 1989). Besides the instabilities that this delicate method involves, it should be noticed that the fact that a substance can actually form threads while being spun (the *spinnability*) is a profound issue in its own right, and some of its ramifications can be seen in (Larson, 1983; Petrie, 2006b). Another important aspect of fibre spinning experiments concerns the history of the strain, which can lead to different responses for different substances.
- Stagnation point flow or opposite jets. In this technique, elongational flow is generated by using a piston or a mill-like device to inject the fluid into a region where orifices are positioned along an axis orthogonal to the entrance direction, so that the sample is forced to separate into opposite elongating jets around the stagnation point (Mackley *et al.*, 1975). The strain rate is controlled by adjusting the flow rate, the radius of orifices and the separation between them, as in the work by Mackay and Dajan (Mackay and Dajan, 1994). The viscous response can be measured via mechanical considerations or using optical methods. In the latter case, light scattering, birefringence and dichroism are instrumental to spatially resolving anisotropies in the flow or molecular alignment. A review and a subsequent book by Fuller (Fuller, 1990, 1997) analyse these and other techniques in depth. Measurements are sensitive to imperfections in the geometry of the flow and material conditions, which can sensibly alter the behaviour of the sample around the stagnation point.
- Converging and contraction flows. The principle of these methods is to drive the sample into an abrupt and rapid contraction by making it flow through a narrower region, using dies of different shapes as in an extrusion process. Evaluating the pressure drop undergone by the fluid and using geometrical considerations on the channel, a calculation of extensional viscosity is possible (Cogswell, 1972b; 1972a; Tremblay, 1989). It is interesting to point out that there is no agreement on the way for calculating viscosity

from these types of experiments, as pointed out in the work by Binding and Gibson (Binding, 1994; Gibson, 1998), and that the flow cannot be considered materially steady.

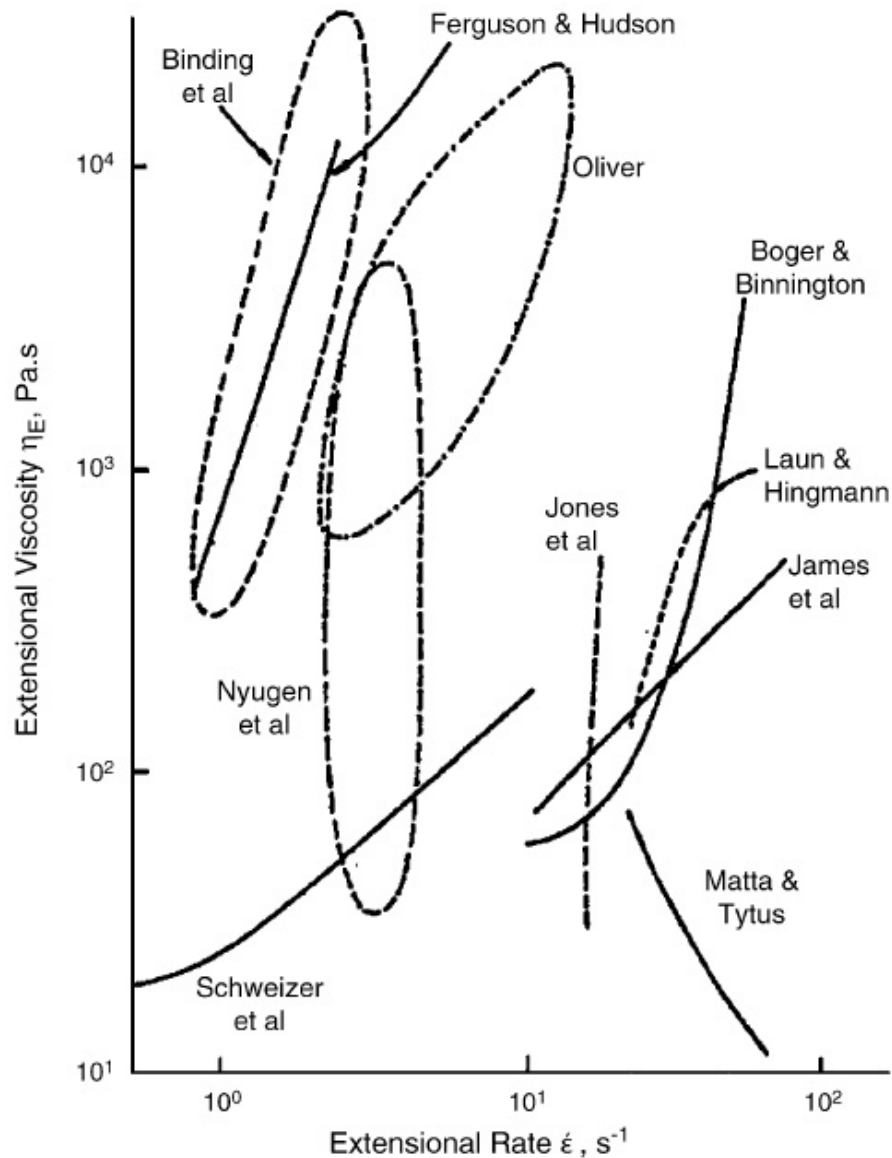


**Figure 2.1. The “M1” muddle: results for steady state elongational viscosity using different techniques are sensitive to the history of the flow and the experimental settings, from (James and Walters, 1994). Details for the experimental settings used by each group can be found in (Petrie, 2006a).**

Finally, let us cite an example to illustrate the dependency of viscosity measurements on experimental conditions and nonlinear properties of the sample under study: a series of

experiments on the polymeric fluid “**M1**”, which have been carried out in laboratories around the globe using all the techniques described above and reported in a special issue of the Journal of Non-Newtonian Fluid Mechanics (see an overview by Sridhar (Sridhar, 1990)). In Fig. 2.1 results by different groups are reported (James and Walters, 1994), showing an almost perfect disagreement among the measurements, which rheologists ironically labelled as the “**M1**” muddle. Nonetheless, the point is that *all* reported results are correct, because different flow histories and incompatibilities in experimental settings generated inconsistent data. *Controllability* of the flow under certain experimental specifications is probably the core problem of extensional rheometry and ultimately stems from the definition (2.1) which, according to Petrie (Petrie, 2006a), “is fine in theory but is a very dangerous idea in practice”. This suggests the utmost care when comparing laboratory data with numerical simulations and constitutive models<sup>1</sup>.

---

<sup>1</sup> We are not concerned with constitutive models for polymers in this Thesis, but the interested reader can find a critical discussion on the limits of those, in light of experimental results for extensional flows, in (Sridhar, 2000).

### ***2.3. The new-cell algorithm for constant pressure simulations.***

A considerable amount of experimental data for the steady-state viscosity of polymer melts and solutions under planar elongational flow is available. Besides the examples that are reported in the previous references, other data can be found in (Laun and Münstedt, 1978; Laun and Schuch, 1989; Greener and Evans, 1998), where the elongational viscosity of polymer melts is extracted from tensile tests; in (Anna *et al.*, 2001; Bach *et al.*, 2003a; Bach *et al.*, 2003b), where the filament stretching technique is employed; in (Laun and Schuch, 1989; Gauri and Koelling, 1997) where fibre-spinning is used; in (Fuller *et al.*, 1987; Gauri and Koelling, 1997) where opposite jets are studied, and in (Laun and Schuch, 1989; Collier *et al.*, 1998; Seyfzadeh and Collier, 2001) where converging and contracting flows are adopted. The work by Arigo and McKinley (Arigo and McKinley, 1998) also presents steady elongational viscosity results, with the use of a falling sphere and optical measurements.

Although the above experimental data are mainly obtained on isothermal samples in equilibrium with atmospheric pressure and whose volumes are changing due to the action of the applied strain, available nonequilibrium molecular dynamics (NEMD) studies on diatomic liquids, alkanes and polymer melts under PEF are carried out in the *NVT* ensemble (Hounkonnou *et al.*, 1992; Matin *et al.*, 2000; Todd, 2001; Daivis *et al.*, 2003; Matin *et al.*, 2003; Baig *et al.*, 2005, 2006). A notable exception is represented by the constant pressure NEMD simulations for a polymer melt performed in (Daivis *et al.*, 2003), where a rescaling of the volume of the simulation cell at the beginning of each nonequilibrium run is implemented, so that the initial pressure of the liquid has the desired value before the accumulation of physical quantities starts. However, even though the density is fixed at a value that corresponds to the required target pressure, the actual simulation is run in the *NVT* ensemble: in the course of the simulation, especially as the rate increases, the pressure does not always remain constant and the difference between the (initial) target pressure and the average liquid pressure is sometimes out of the error range of the former (Matin, 2002).

To bridge this gap, an algorithm implementing the Nosé-Hoover integral feedback mechanism for pressure is described and applied to a simple atomic liquid. The fact that

simple liquids display a wide range of non-Newtonian phenomena has been established for more than twenty years (Evans *et al.*, 1984; Hoover, 1984) and there is a significant literature on them. Some of the early examples of the calculation of viscoelasticity of simple liquids under shear include those where a field-driven NEMD approach is used (Ashurst and Hoover, 1975), and those where the DOLLS algorithm is employed (Hoover *et al.*, 1980; Evans, 1981; Heyes *et al.*, 1983; Evans and Morriss, 1984). Other, more recent studies for atomic liquids under steady shear can be found in (Ryckaert *et al.*, 1988; Evans *et al.*, 1989; Ferrario *et al.*, 1991; Travis *et al.*, 1998) and a detailed treatment of the behaviour of viscosity at low shear rates is given in (Borzak *et al.*, 2002), where the use of the transient time correlation function formalism, which has a larger signal-noise ratio than direct time-averaging NEMD in that regime, is adopted. For elongational flows, the implementation of Kraynik-Reinelt periodic boundary conditions discussed in Subsection 1.3.4, has dramatically improved the length of simulations, but, before their introduction, non-Newtonian behaviour was investigated in (Heyes, 1985, 1986; Evans and Heyes, 1990), and results from improvements in simulations length were presented in (Pierleoni and Ryckaert, 1991; Baranyai and Cummings, 1995). Confirmations of the dependency of viscosity on elongational rate can also be found in (Todd and Daivis, 1997; Daivis and Todd, 1998) where the imposition of an oscillating elongational field avoids the limitation of simulation lengths in steady-state regimes. After the introduction of KR pbc, further studies have strengthened previous findings and improved their accuracy (Baranyai and Cummings, 1999; Matin *et al.*, 2000).

A consideration of the lattice cell evolution for PEF is necessary each time the volume change, inherent to the NH mechanism, takes place. This aspect has not been crucial in analogous studies for planar shear flow as, for instance, sliding brick pbc are applied on a unit cell that does not change shape. According to the observations presented in subsections 1.3.5 and 1.3.6, which we will refer to in the following, the adjustment of the boxlengths needed for the NH barostatting procedure for PEF, Eq. (1.38), must be implemented without jeopardising the dynamics of particles in the unit simulation lattice and with no alteration of the angle  $\theta(t)$  (see Eq. (1.31)) between the  $x$  and  $y$  dimensions  $\mathbf{L}_1(t)$  and  $\mathbf{L}_2(t)$  (see Fig. 2.2). Three possible strategies are presented below, with particular details for the *new-cell* method, which is then used for nonequilibrium viscosity calculations.

In three dimensions, the first possible (and straightforward) method is given by only rescaling the  $z$  dimension of the simulation box, which has no influence on the evolution of  $\mathbf{L}_1(t)$  and  $\mathbf{L}_2(t)$  that takes place in the  $xy$  plane (see Eq. (1.29)). In this case, if the elongational rate, the pressure and/or the density are very high, rescaling only the  $z$  dimension could be risky, as the distance between particles in that direction might become too short and cause a violation of the minimum image convention.

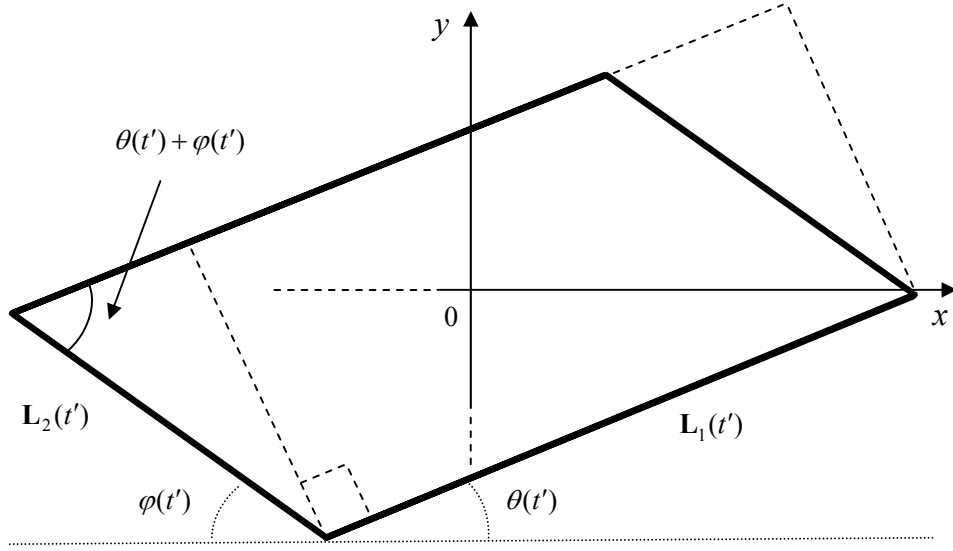


**Figure 2.2.** The volume of the tilted lattice at a time  $t'$  is given by the area of the  $xy$  parallelogram, i.e.  $\|\mathbf{L}_1(t')\| \cdot \|\mathbf{L}_2(t')\| \sin(\theta(t') + \varphi(t'))$ , multiplied by the length of the  $z$  dimension (orthogonal to the page). Multiplying the modulus of each dimension  $\mathbf{L}_i(t')$  by the factor  $\lambda$  given by Eq. (2.2) gives the target value for the volume according to Eq. (1.38) and preserves the angles  $\theta(t')$  and  $\varphi(t')$ . The  $xy$  plane section is shown.

An alternative solution consists in the application of the appropriate contraction/dilation factor to all three lattice dimensions. We indicate with  $V_T(t')$  the solution of Eq. (1.38) at timestep  $t'$ :  $V_T(t')$  is the target volume that maintains the average pressure at its target value  $p_0$  given in Eq. (1.41). If  $V(t')$  is the unrescaled cell volume, i.e.  $V(t') \neq V_T(t')$ , then the rescaling factor at  $t'$  is given by

$$\lambda(t') = \left[ \frac{V_T(t')}{V(t')} \right]^{1/3} \quad (2.2)$$

There are two equivalent ways of using this factor to produce the appropriate unit cell.

The first one naturally involves the direct rescaling of the tilted elongated cell, such that the lattice vector moduli  $\|\mathbf{L}_i(t')\|$  are replaced as follows:  $\|\mathbf{L}_i(t')\| \rightarrow \lambda(t')\|\mathbf{L}_i(t')\|$ , where  $i = 1, 2, 3$  indicates the  $x, y$  and  $z$  direction. The volume of the tilted box at time  $t'$  is given by  $\|\mathbf{L}_1(t')\| \cdot \|\mathbf{L}_2(t')\| \cdot \|\mathbf{L}_3(t')\| \sin(\theta(t') + \varphi(t'))$  (see Fig. 2.2) and the rescaling clearly leads to the correct volume  $V_T(t')$  solution of Eq. (1.38) with no alteration in the angles  $\theta(t')$  and  $\varphi(t')$ .

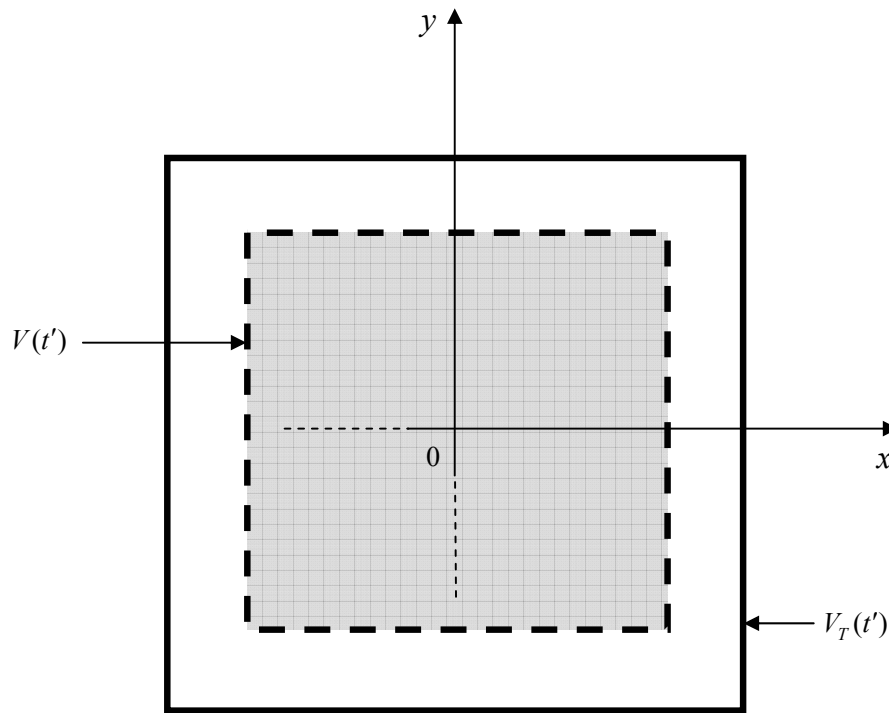


**Figure 2.3. Step 1 of the *new-cell* rescaling procedure: a “new” cubic cell is created, with the appropriate volume  $V_T(t')$  given by Eq. (1.38).**

The second way does not deal directly with the tilted cell, but uses an initial “new” cubic cell with volume  $V_T(t')$  and the evolution equations (1.29) to obtain the appropriate simulation cell. A three step procedure to produce the proper tilted cell with volume  $V_T(t')$  is possible. First, a “new” cubic unrotated cell with volume  $V_T(t')$  is generated (see Fig. 2.3). This cell has three equal  $x, y$  and  $z$  sides of length  $(V_T(t'))^{1/3}$ . Second, a rotation of the

initial KR angle  $\theta_0$  (see Subsection 1.3.4) is performed on this cell (Fig. 2.4). Finally, to recover the correct tilted dimensions at time  $t'$ , the “new” target cell is evolved via Eqs. (1.29):

$$\begin{aligned} {}^{new}L_{T,ix}(t') &= {}^{new}L_{T,ix}^0 \exp(\hat{\epsilon}t') \\ {}^{new}L_{T,iy}(t') &= {}^{new}L_{T,iy}^0 \exp(-\hat{\epsilon}t') \end{aligned} \quad (2.3)$$

where  ${}^{new}\mathbf{L}_{T,1}^0$  and  ${}^{new}\mathbf{L}_{T,2}^0$  are the vectors of the “new” cubic cell with length  $(V_T(t'))^{1/3}$  which has been rotated by an angle  $\theta_0$  with respect to the  $x$ -axis as indicated in Fig. 2.4.

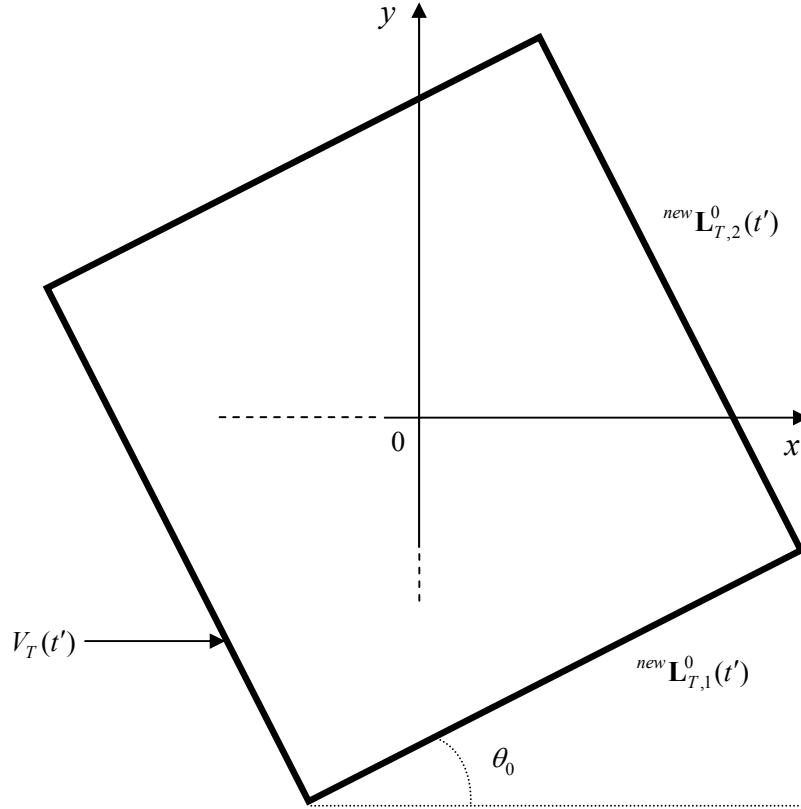


**Figure 2.4.** Step 2 of the *new-cell* rescaling procedure: the “new” cubic lattice is rotated in counter clockwise direction by the initial angle  $\theta_0$ .

The tilted cell given by  ${}^{new}\mathbf{L}_{T,1}(t')$  and  ${}^{new}\mathbf{L}_{T,2}(t')$  is the same cell given by the previous method with homogeneous rescaling: it has the correct volume  $V_T(t')$ , as the evolution Eqs. (1.29) conserve the cell volume, and the angle  $\theta(t')$  is preserved. In fact, according to Eq.

(1.31),  $\theta(t')$  depends only on the initial (rotated) lattice components  $L_{1x}(t=0)$  and  $L_{1y}(t=0)$ . The procedure rescales the (unrotated) lattice vector  $\mathbf{L}_1(t=0)$  by the factor  $\lambda(t')$ , preserving the ratio of its  $y$  and  $x$  components (see Fig. 2.5). An explicit calculation of the volume for the new cell gives:

$$\begin{aligned} {}^{new}V(t') &= \|{}^{new}\mathbf{L}_{T,1}(t')\| \cdot \|{}^{new}\mathbf{L}_{T,2}(t')\| \cdot \|{}^{new}\mathbf{L}_{T,3}(t')\| \sin({}^{new}\theta(t') + {}^{new}\varphi(t')) \\ &= \lambda(t') \|\mathbf{L}_1(t')\| \cdot \|\mathbf{L}_2(t')\| \cdot \|\mathbf{L}_3(t')\| \sin(\theta(t') + \varphi(t')) \\ &= \lambda(t') V(t') = V_T(t') \end{aligned}$$

When the next rescaling is necessary at a time  $t'' > t'$ , the procedure is repeated creating a “new” initial lattice with a volume  $V_T(t'')$  given by Eq. (1.38) solved at time  $t''$ , using a new  $\lambda(t'')$  with  $V_T(t'')$  and the current unrescaled volume  $V(t'')$ . This procedure is then repeated throughout the time evolution of the simulation.

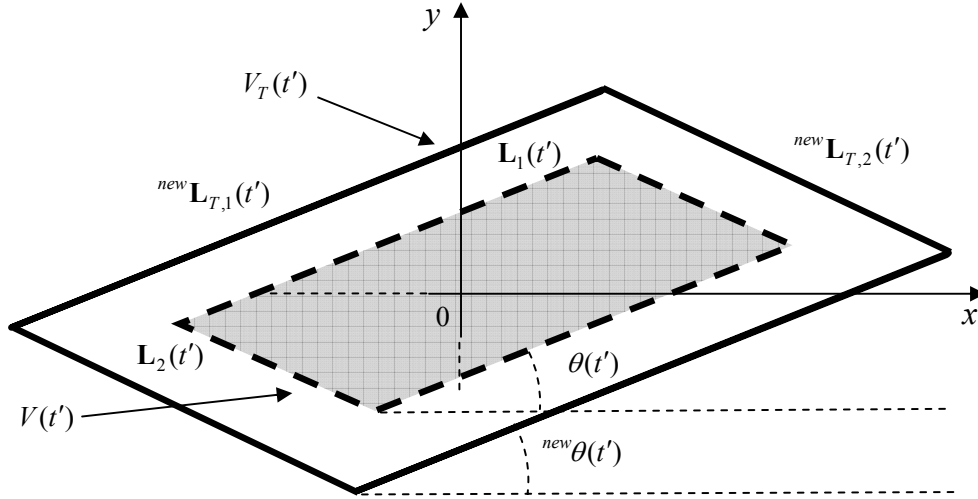


**Figure 2.5. Step 3 of the *new-cell* rescaling procedure: the created lattice is evolved to the same instant  $t'$  when the rescaling process takes place.  ${}^{new}\mathbf{L}_{T,1}(t')$  and  ${}^{new}\mathbf{L}_{T,2}(t')$  are the new tilted vectors, which correspond to a lattice with the proper volume  $V_T'$  given by Eq. (1.38). The current angle  ${}^{new}\theta(t')$  is the same as it was for the previous unrescaled lattice  $\theta(t')$  with volume  $V(t')$ . In the case of volume contraction, the procedure is the same and the resulting “new” lattice has a volume  $V_T(t') < V(t')$ . The application of pbc's after the integration of the equations of motion ensures that if any particle is out of the “new” cell boundaries, it is properly mapped back into it.**

Since the two methods produce the same target cell and entail a comparable amount of computation, the choice of implementation is left to the user, depending on how the KR conditions are coded. Some readers may use programs that compute the lattice vector moduli as  $t$  evolves and prefer the first method, whereas others, like us, may choose to evolve the vector components only (Eqs. (1.29)) and are therefore interested in the second method which does not require the calculation of vector moduli.

In both approaches, during every rescaling process the particles are obviously unmoved, and pbc's are imposed on the rescaled cell at the end of each contraction/dilation procedure, after the integration of the equations of motion (1.38), (1.39) and (1.41). Thus, any particle out of the boundaries is properly mapped back into the rescaled unit lattice via the application of standard pbc's.

To test our *new-cell* procedure, simulations for a 3-dimensional system of 2048 atoms undergoing PEF are performed. The atoms interact via the WCA potential and, using reduced units, the system is kept at a constant temperature  $T = 1.00$  and has an initial density  $\rho = 0.840$ . The pressure for the nonequilibrium  $NpT$  simulations is set at the value obtained from an equilibrium simulation at constant volume and temperature ( $NVT$ ), that for this system is  $p_0 = 7.8365 \pm 0.0001$ .

A fourth order Gear predictor-corrector scheme is used to integrate the equations of motion. The timestep is  $\Delta t = 0.001$  for all the elongational rates, except the two highest ones ( $\dot{\epsilon} = 3.5$  and  $\dot{\epsilon} = 5.0$ ), where the timestep is reduced to  $\Delta t = 0.0002$  to maintain good accuracy. Data are collected from three independent runs starting from a fcc lattice for all rates, with initial momenta for the atoms randomly chosen. The pressure is conserved, on average, within 0.01% of its nominal value in almost all the cases and has a maximum inaccuracy of about 0.1% in the case of the highest rates (see Table 2.1 for details).

The choice of the damping factor is  $Q = 300$ : as the total length of the simulation for every elongational rate is 15 millions timesteps, the average of viscosity is taken over a sufficient number of pressure oscillations, in accordance with the observations presented in Section 1.3.

It is worthwhile running a number of checks on the algorithm to rule out any possible inadequacy caused by the pressure conservation mechanism. No violation on conservation properties or discontinuity in the physical variables has ever been observed. For example, simulations show expected results at equilibrium and out of equilibrium when the thermostat is turned off, no ‘jump’ in any thermodynamic or transport quantities occurs when the reshaping of the unit cell is carried out, and no rate-dependent artificial effect of any kind is seen in the KR conditions.

Also, as the initial density and the pressure of the sample are not very high, the strategy involving the compression/dilation only in the  $z$  direction can also be used: it is found that results for the two methods agree within statistical uncertainty. From the theoretical point of view, it is also important to appreciate that the validity of the method we propose is unaffected by the type of thermostat used, and works either with the NH or the Gaussian formulation. As we explained in Section 1.2, the two formulations give rise to equal steady-state averages (Evans and Sarman, 1993), and our choice of the latter ultimately stems from its better efficiency in computing viscosity coefficients for liquids out of equilibrium (Evans and Holian, 1985).

Moreover, it is important to bear in mind that the present *algorithm* for  $NpT$  simulations of elongational flow is primarily intended for use either in simulations of molecular fluids, where the onset of viscoelastic effects indeed occurs at weaker and experimentally reproducible rates of strain as the size of molecular chains increases, and for the theoretical calculations on the chaotic properties for simple atoms under this kind of dynamics, as it will be explained in Chapters 3 and 4. Hence, our validation is performed on an atomic fluid in the same way as the implementation of the  $NpT$  algorithm for constant shear flow was first performed for a soft-sphere liquid (Hood *et al.*, 1989) and then later straightforwardly applied for more complex molecular systems (Daivis and Evans, 1994).

In Fig. 2.6, the values of elongational viscosity for the  $NpT$  and the  $NVT$  ensembles are plotted, where, for the  $NVT$  case, simulations at constant  $V$  are run. This type of comparison does not take equivalent state points into account, because, in the extended space of thermodynamic variables  $(p, T, V, \dot{\epsilon})$  (Evans and Baranyai, 1991; Daivis and Evans, 1994),

points at different  $\dot{\epsilon}$  are respectively reached via an isobaric and an isochoric transformation for  $NpT$  and  $NVT$  regimes. If we use the final pressure  $p$  of a  $NVT$  simulation at a given  $\dot{\epsilon}$  and run an  $NpT$  simulation at the same  $p$ , results for viscosity are the same in both ensembles. This will also be explicitly confirmed for smaller systems in Section 4.3.

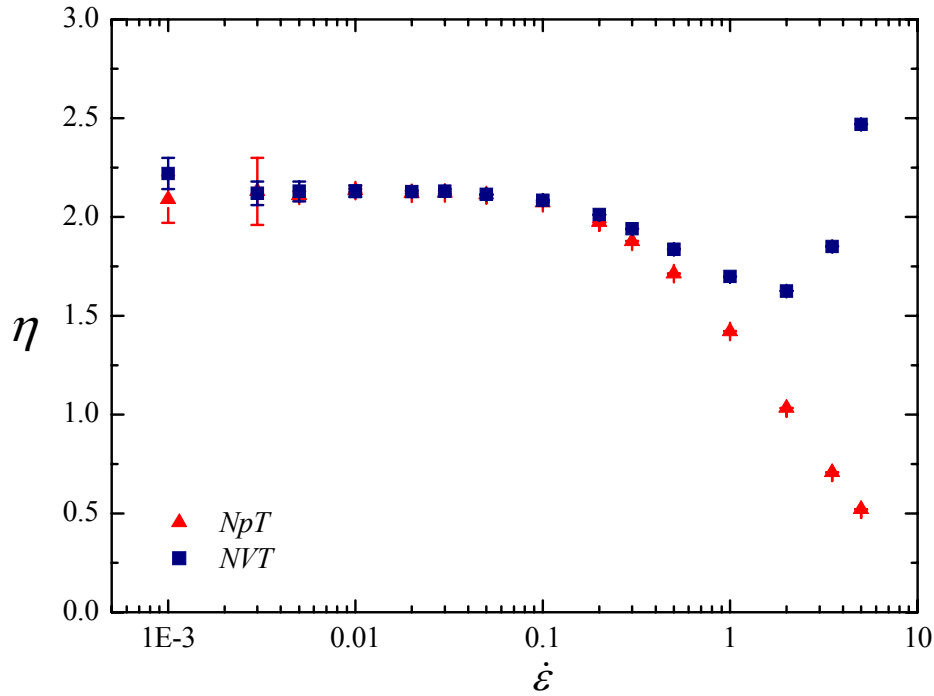


**Figure 2.6. Planar elongational viscosities for the isokinetic-isochoric ( $NVT$ ) and isokinetic-isobaric ( $NpT$ ) ensembles as functions of the elongation rate  $\dot{\epsilon}$ .**

Viscosities for constant pressure and constant volume regimes are within statistical errors of each other until  $\dot{\epsilon} \leq 0.3$ , after which they diverge: these results for an atomic liquid show a behaviour similar to previously reported NEMD simulations of complex liquids, confirming that the algorithm is consistent. Two well-known ensemble-dependent trends for  $\eta(\dot{\epsilon})$  at high rates, namely elongational thinning and thickening, are apparent.

In general, a decrease in viscosity with strain rate (i.e. thinning) for atomic liquids is an effect caused by the distortion of nearest neighbour shells due to the external field (Marcelli *et al.*, 2001), whereas for complex liquids is a combination of this and changes in molecular alignment (Hess, 1983; Davis and Evans, 1994). There also exists some recent

experimental evidence of this mechanism for atomic liquids under shear in (Berg *et al.*, 1999; Berg, 2004), where, although for a different state point than the one investigated here, it is shown that viscoelasticity occurs in atomic liquids at constant temperature and constant pressure. The higher rates in Fig. 2.6, where the elongation-dependant behaviour is more marked, have not yet been experimentally reproduced and are currently difficult to access, as, for instance, they correspond to an elongation rate of order  $10^{12}$  Hz for liquid Argon. This is far too high compared with available experimental techniques: cutting-edge experiments on aqueous polymer solutions confined in microchannels have recently reproduced a maximum shear rate as high as  $10^6$  Hz (Kang *et al.*, 2005).

**Table 2.1. Simulation results for  $NpT$  and  $NVT$  viscosity and pressure at different elongation rates. Uncertainties are at  $2\sigma$  where  $\sigma$  is the standard error, and are next to the relevant significant figure. It is evident that the signal-to-noise ratio dramatically decreases as  $\dot{\epsilon}$  approaches zero.**

$\dot{\epsilon}$	$NpT$		$NVT$	
	$\eta$	$p$	$\eta$	$p$
0.001	2.1(1)	7.8365(1)	2.22(8)	7.8365(4)
0.003	2.1(2)	7.8364(1)	2.12(6)	7.8364(4)
0.005	2.11(2)	7.8364(1)	2.13(5)	7.8366(4)
0.01	2.133(8)	7.8365(1)	2.13(3)	7.8369(4)
0.02	2.12(1)	7.8364(1)	2.128(8)	7.8380(3)
0.03	2.121(9)	7.8365(1)	2.13(1)	7.8398(1)
0.05	2.112(1)	7.8364(1)	2.115(2)	7.8459(4)
0.1	2.073(1)	7.8365(1)	2.084(2)	7.8722(2)
0.2	1.973(1)	7.8365(1)	2.012(1)	7.9610(1)
0.3	1.877(1)	7.8365(1)	1.942(1)	8.0832(4)
0.5	1.7136(4)	7.8367(1)	1.8369(7)	8.398(1)
1.0	1.4216(2)	7.8370(1)	1.6982(2)	9.5303(1)
2.0	1.0329(1)	7.839(1)	1.6257(2)	13.333(1)
3.5	0.7076(1)	7.841(1)	1.8508(8)	24.31(1)
5.0	0.5218(1)	7.845(2)	2.469(1)	46.23(2)

---

In the case of constant volume simulations, a strain hardening mirrors the so-called shear-thickening effect for shear, i.e. an increasing viscosity for increasing strain rate. This behaviour is peculiar to the nature of  $NVT$  dynamics and, in the case of shear flow, is accompanied by instabilities in the flow profile and asymmetric contributions in the normal stress coefficients (Delhommelle, 2004b). The fact that some authors have not reported this effect for molecular systems is due to an erroneous implementation of the molecular constraint on temperature, which promoted an unphysical molecular alignment and consequent artificial decrease in viscosity, as discussed in (Travis *et al.*, 1995b, 1995a, 1996). The thickening transition has been experimentally confirmed, for instance, in colloidal suspension and polymer dispersions under shear (Newstein *et al.*, 1999; Maranzano and Wagner, 2001, 2002) and elongation (O'Brien and Mackay, 2002; Ascanio *et al.*, 2006; Sosa *et al.*, 2006). Although it is clear that high viscosities for atomic fluids at  $NVT$  are due to a faster increase in the stress with respect to shear or elongational rates (see Table 2.1), an explanation at particle level is still not available, even though progresses have been made in recent years by means of ideas like contact networks (Melrose *et al.*, 1996; Melrose, 2003) and jamming (Cates *et al.*, 1998).

Because of the differences in the two regimes, an  $NVT$  simulation eventually fails to match the experimental results and this is also why we have to resort to  $NpT$  methods. The *new-cell* procedure is an accurate, easy to implement and self-starting option to realize this.

We conclude this Chapter with an observation. Results for viscosity from  $NVT$  simulation of PEF seems not to show the onset of a string phase. On the contrary, recent results showed that the viscosity of Gaussian isokinetically constrained WCA atomic fluids either under shear (Delhommelle, 2003; Delhommelle, 2004a) or under a color field (Delhommelle, 2005) displays a dramatic drop approximately from  $\dot{\gamma} \sim 2.0$  to  $\dot{\gamma} \sim 10.0$ , after which a pathological oscillating regime is found. This behaviour disappears when a configurational thermostat is employed: making no assumptions on the flow profile results in the appearance of thickening at  $\dot{\gamma} \sim 5.0$  after the expected decrease in  $\eta(\dot{\gamma})$  for smaller rates. This latter trend resembles Fig. 2.6 very closely, as  $\eta(\dot{\epsilon})$  has a similar gradual decline before  $\dot{\epsilon} \sim 2.5$  and then an immediate appearance of thickening. Curiously,  $\dot{\epsilon} \sim 2.5$  gives approximately the same energy dissipation  $\Pi$  (see Section 4.2.1 and (Bird *et al.*,

1987)) as  $\dot{\gamma} \sim 5.0$ , even though data are obtained at different state points. Of course this observation is far from being an actual proof, and it would be interesting to conduct an inspection on the spatial distribution of particles and a comparison of the present results for PEF with runs using a configurational thermostat in the future. We will also return on this in Subsection 4.4.2, from a different perspective.